Journal of Inorganic Biochemistry xxx (xxxx) 112686

Contents lists available at ScienceDirect

Journal of Inorganic Biochemistry

journal homepage: www.elsevier.com/locate/jinorgbio

Heme pocket hydrogen bonding residue interactions within the *Pectobacterium* Diguanylate cyclase-containing globin coupled sensor: A resonance Raman study

Nushrat J. Hoque [a], Shannon Rivera [b, 1], Paul G. Young [b, 1], Emily E. Weinert [a, c, *], Yilin Liu [d, **]

[a] Department of Chemistry, Pennsylvania State University, University Park, PA 16802, USA
[b] Department of Chemistry, Emory University, Atlanta, GA 30322, USA
[c] Department of Biochemistry and Molecular Biology, Pennsylvania State University, University Park, PA 16802, USA
[d] Department of Chemistry, University of Akron, Akron, OH 44325, USA

ARTICLE INFO

Keywords:
Heme
Resonance Raman
Oxygen sensing
Globin
Diguanylate cyclase

ABSTRACT

Heme-based sensor proteins are used by organisms to control signaling and physiological effects in response to their gaseous environment. Globin-coupled sensors (GCS) are oxygen-sensing proteins that are widely distributed in bacteria. These proteins consist of a heme globin domain linked by a middle domain to various output domains, including diguanylate cyclase domains, which are responsible for synthesizing *c*-di-GMP, a bacterial second messenger crucial for regulating biofilm formation. To understand the roles of heme pocket residues in controlling activity of the diguanylate cyclase domain, variants were characterized by enzyme kinetics and resonance Raman spectroscopy. Results of these studies have identified roles for hydrogen bonding and heme edge residues in modulating heme pocket conformation and flexibility. Better understanding of the ligand-dependent GCS signaling mechanism and the residues involved may allow for future development of methods to control O_2-dependent *c*-di-GMP production.

1. Introduction

Heme sensor proteins are widely distributed in nature, from bacteria to mammals, and are characterized by containing both a functional domain and a heme-containing sensor domain capable of binding diatomic gas molecules like O_2, CO, and NO [1–3,4,5]. In general, binding of these ligands to the heme induces conformational changes at the active site, which are transmitted to the protein's functional domain, thereby regulating physiological effects of various biological systems [5–8]. Globin-coupled sensor (GCS) proteins are an important class of heme-containing proteins proposed to serve as in vivo O_2 sensors and are predicted in the genomes of ~1000 bacterial species [9–12]. GCSs consist of a N-terminal heme globin domain, linked by a variable middle domain to a variety of output domains, such as methyl accepting chemotaxis proteins (MCP; involved in motility) [13–15], kinases [16–18], diguanylate cyclases (DGC; synthesize cyclic di-GMP (*c*-di-GMP), a bacterial second messenger) [19–23], phosphodiesterases (EAL or HD-GYP; hydrolyze *c*-di-GMP) [24,25], and gene regulatory proteins (Fig. 1A).

GCS proteins containing DGC output domains, characterized in *E. coli* (*Ec*DosC) [20,21,26,27], *Pectobacterium carotovorum* (*Pcc*GCS) [19,28–31], and *Shewanella* species [22,32], among others [3,24,33], play a pivotal role in regulating the intracellular concentration and signaling of the second messenger *c*-di-GMP (Fig. 1B) [34]. DGC domains (also termed GGDEF for the active site residues) cyclize two molecules of guanosine triphosphate (GTP) to form *c*-di-GMP, as well as two molecules of inorganic pyrophosphate (PPi) (Fig. 1C). As *c*-di-GMP regulates many bacterial processes, including biofilm formation, motility, and virulence [35–38], it is important to understand the mechanism by which oxygen binding controls *c*-di-GMP production in GCSs. While previous studies have demonstrated that ligand binding to the heme modulates diguanylate cyclase activity within DGC-containing GCSs [39,3,21,32,40,41], a major obstacle in understanding the regulatory mechanism is the lack of comprehensive structural information for GCS proteins and the differences observed for GCSs from different species.

* Corresponding author at: Department of Chemistry, Pennsylvania State University, University Park, PA 16802, USA.
** Corresponding author.
E-mail addresses: emily.weinert@psu.edu (E.E. Weinert), yliu1@uakron.edu (Y. Liu).
[1] These authors contributed equally to this work.

https://doi.org/10.1016/j.jinorgbio.2024.112686
Received 30 March 2024; Received in revised form 23 July 2024; Accepted 29 July 2024
0162-0134/

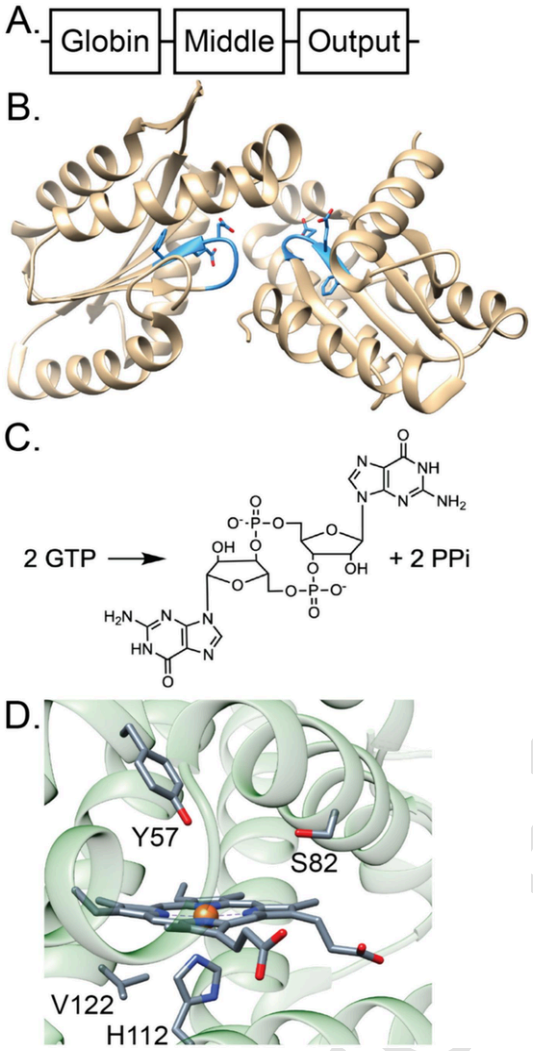

Fig. 1. PccGCS domain architecture (A.), diguanylate cyclase domain dimer (PDB: 4URG; B.)[34], catalyzed reaction (C.), and heme pocket residues under investigation (D.).

Consequently, identifying the roles of essential residues in the active site, responsible for conformational change and signal transduction and comparing between homologous GCS proteins is of interest, as the studies can provide new insights. Understanding the mechanism of signaling events that lead to the activation or deactivation of these biological process will allow us to understand how cells adapt to environmental changes and potentially highlight methods to disrupt the signaling mechanism.

Among the many diverse spectroscopic methods, resonance Raman (rR) spectroscopy has proven itself to be a highly effective tool to detect the structures of heme proteins and their intermediates [42]. This technique enables the selective amplification of heme vibrational modes by tuning the excitation wavelength to closely match the heme absorption bands [43,44]. Information on the oxidation and spin states of heme iron is easily accessible through specific "marker modes" present in the high wavenumber segment of the vibrational spectrum. The low wavenumber segment offers valuable insights into the interactions between protein residues and the peripheral heme groups, such as the vinyl and propionate substituents. This information is crucial for documenting the interaction between these peripheral groups and the protein; it can elucidate the structural effects resulting from heme-ligand binding, thereby dictating the heme's reactivity [45–47]. Significantly, this method proves especially beneficial in studying the alterations in the positioning of exogenous axial ligands due to substrate binding, as well as in investigating variations within the active site environment. This includes assessing changes in distal pocket polarity and steric interactions that are introduced by the substrate or specific amino acid residues [48].

In the present study, enzyme activity assays and rR spectroscopy are used to probe the effects of key active site variants of the *P. carovotorum* GCS (*Pcc*GCS) and the *Pcc*GCS heme domain (*Pcc*Globin), as well as to compare the full-length *Pcc*GCS to the isolated globin domain using CO as a probe. The two distal pocket hydrogen bonding residues (Y57 and S68) were chosen based on previous studies on the globin domains of *Pcc*GCS and *Bpe*GReg that identified both residues as important in stabilizing O_2 binding (Fig. 1D). In addition, distal pocket hydrogen bonding residues have been demonstrated to be important in both ligand binding and output domain activation for other GCS proteins, such as those from *Escherichia coli* (*Ec*DosC) [40], *Bacillus subtilis* (HemAT-*Bs*) [14], and *Anaeromyxobacter* sp. Fw109–5 (*Af*GcHK) [17]. Mutation of the proximal histidine was performed to determine if the covalent linkage between proximal ligand and the protein was required for stable O_2 binding, while the Val122 position was investigated due to the van der Waals contacts with the heme [49], suggesting that it may be involved in tuning heme electronics.

Results from these studies have highlighted the importance of heme pocket residues in modulating ligand-dependent cyclase domain activation, selectivity of ligand activation, and changes to heme conformation, hydrogen bonding, and electronics. Alterations observed in the frequencies and intensities of modes related to the Fe-C-O fragment offer valuable insights into the polarity of the distal pocket environment, highlighting potential hydrogen-bond interactions with distal amino acids, water molecules, or substrates. The results of these studies provide insights into how heme pocket hydrogen bonding interactions modulate diguanylate cyclase domain activity within the GCS family, which will allow for improved predictions of GCS functions in vivo.

2. Experimental

2.1. Protein expression

Site-directed mutagenesis was performed on a codon-optimized gene encoding *Pcc*GCS or PccGlobin within a pET-20b vector [50]. Protein variants were generated by standard PCR protocol as previously described [29]. Proteins, both full-length and globin domain (using a plasmid encoding only the globin domain), were expressed in *E. coli* Tuner (DE3) pLysS cells (Novagen) as previously described [28,29]. Briefly, cells were transformed with pET20b plasmids encoding each protein via heat shock, then grown overnight on LB agar plates containing chloramphenicol (30 μg /mL) and ampicillin (100 μg /mL). Plates were re-streaked and single colonies were selected and grown overnight at 37 °C with shaking at 225 rpm in lysogeny broth (LB) medium with appropriate antibiotics for selection. These overnight cultures were then used to inoculate globin expression media (45 g yeast extract, 10 mL glycerol, 2.31 g anhydrous KH_2PO_4, 16.4 g anhydrous K_2HPO_4 per 1 L of ultrapure water). The inoculated cultures were incubated at 37 °C with shaking at 225 rpm until they reached an OD_{600} of 0.6–0.8. At this point, the temperature was decreased to 25 °C and δ-aminolevulinic acid was added at a final concentration of 500 μM to each expression mixture. Cultures were incubated with shaking for 30 min, at which point protein expression was induced by addition of 100 μM IPTG for 6 h. Cells were then harvested by centrifugation (3500 x*g*, 4 °C, 20 min) and the resulting pellets were collected and stored at −80 °C.

2.2. Protein purification

Low imidazole buffer (50 mM Tris, 30 mM NaCl, 20 mM imidazole, 5% glycerol (*v*/v), pH 7.4) was used to resuspend cell pellets, which were then lysed using a homogenizer (Avestin) or a sonicator (Qsonica), and partially purified by centrifugation (186,000 x*g*, 4 °C, 1 h). The resulting supernatant was then loaded onto an equilibrated HisPur Ni^{2+}-column (Fisher Scientific) and washed with low imidazole buffer. The protein was eluted using high imidazole buffer (50 mM Tris, 30 mM NaCl, 1 mM DTT, 250 mM imidazole, 5% glycerol (*v*/v), pH 7.4) and, following elution, proteins were further purified and desalted with a S200 gel filtration column (50 mM Tris, 50 mM NaCl, 1 mM DTT, 5% glycerol (v/v), pH 7.0). Protein-containing fractions were then concentrated by ultrafiltration (10 kDa MWCO filter, Millipore), aliquoted, flash frozen in liquid nitrogen, and stored at −80 °C. His-tags were not cleaved from the proteins as earlier studies [39] found that removal of the affinity tag didn't change O_2 dissociation rates or enzyme kinetics. The molecular weight, including His-tag and linker, of full-length *Pcc*GCS is 54.8 kDa and of *Pcc*Globin is 21.5 kDa (Fig. S1). All of the variants yielded stable protein that remained heme bound through purification, thawing to perform kinetics/spectroscopy, and during the assays.

2.3. Michaelis-Menten enzyme kinetics

Proteins were reduced and various protein ligand complexes were formed prior to kinetic assays as previously described [39,51]. Ligation states were verified for each protein via UV–vis spectroscopy prior to each assay (Fig. S2) [52]. All Fe(II) and Fe(II)-NO kinetic rates were measured in an anaerobic chamber (Coy) using a Biotek Epoch2 plate reader within the anaerobic chamber, anaerobic buffers, and an EnzChek kit that was prepared and stored on a chilling block within the anaerobic chamber. In order to measure the rates of DGC output from the DGC-GCS proteins, the EnzChek pyrophosphate kit (Life Technologies) was used according to the manufacturer's instructions, the exception being that *a* phosphodiesterase (PDE) *Ec*DosP was added in 3-M excess to eliminate product inhibition [53] and the reactions were initiated by the addition of varying concentrations of GTP. Assays were performed in triplicate in 96-well plates with 4 protein concentrations (0, 0.5, 1, and 2 μM) and 4 GTP concentrations (0, 100, 250, and 1000 μM) and were monitored using an Epoch or Epoch2 plate reader and Gen5 software (Biotek) and repeated at least twice to account for day-to-day variability.

2.4. Stopped-flow kinetics

O_2 dissociation rates were performed as previously described [29,54]. Briefly, all proteins were reduced with dithionite in an anaerobic chamber (Coy), desalted into anaerobic Buffer A (50 mM Tris, 50 mM NaCl, pH 7.0), and then mixed with O_2 saturated Buffer A to yield final concentrations of 5–10 μM. Protein samples were rapidly mixed with a solution of sodium dithionite in Buffer A (final dithionite concentration = 5 mM; dithionite concentration of 0.5 mM also was tested and dithionite concentration was found to not affect the O_2 dissociation rate) in an SX20 stopped flow apparatus. The dissociation of O_2 performed at 25 °C was monitored using the SX20 stopped flow equipped with a diode array detector and temperature-controlled bath and fit globally using Pro-KII software (Applied Photophysics). Additional fitting analysis was performed using Igor Pro (Wavemetrics).

2.5. Resonance Raman sample preparation

Samples of the GCS proteins, produced through the procedures described above, were prepared for resonance Raman (rR) spectroscopy measurements. To prepare the deoxygenated samples, *Pcc*GCS WT (full-length) and *Pcc*Globin (only globin domain) WT, Y57F, S82A and V122Y (~100 μL of 120 μM) were placed in NMR tubes (WG-5 M-ECONOMY-7, Wilmad Glass Co., Beuna, NJ), connected to a vacuum line and degassed followed by saturation with argon gas. This procedure was repeated twice. Sufficient dithionite solution was added to fully reduce the samples, the formation of ferrous form was confirmed by monitoring the Q region of electronic absorption spectrum, using a device (ISS-2 integrated sampling system, Ocean Optics Inc) that can measure spectra for the NMR tubes connected to vacuum line. The carbon monoxide complexes of the ferrous *Pcc*GCS heme domain, including both the wild type and variants, were generated using the CO ligand. Specifically, 100 μL of 150 mM *Pcc*GCS (heme domain) samples of the wild type and the variants, as well as the full length of *Pcc*GCS wild type, were transferred into NMR tubes, then sealed with a rubber septum. The CO gas was introduced to the solution using a long needle for 20 min to remove oxygen. Then samples were reduced with a 2-fold excess of degassed sodium dithionite solution and CO gas was further bubbled for an additional 10 min before measuring the rR spectra.

2.6. Resonance Raman measurements

Resonance Raman (rR) spectroscopy was employed to analyze alterations in heme conformation and properties in *Pcc*GCS WT and *Pcc*Globin WT, Y57F, S82A and V122Y. The rR spectra of ferrous samples were measured with 441.6 nm excitation line from a He—Cd laser (1 K Series He—Cd laser, Kimmon Koha., Ltd), while the ferrous CO adducts were measured with the 413.1 nm excitation line, which is from a Kr + laser (Coherent Innova Sabre Ion Laser). All spectra were measured using a Spex 1269 spectrometer equipped with a Spec-10 LN liquid nitrogen-cooled detector (Princeton Instruments, NJ). For data collection, backscattering (180°) geometry was utilized, and the laser beam was focused by a cylindrical lens to create a line image on the sample, reducing the risk of heating and minimizing photodissociation. The laser power incident on the ferrous samples was maintained at ~10 mW, while being adjusted to 1 mW or less on the ferrous-CO samples. The slit width was 150 μm and the 1200 g/mm grating was used for measurements. Spectra were calibrated with data acquired for fenchone and processed with Grams/32 AI software (Galactic Industries, Salem, NH).

3. Results and discussion

Previous work has established that DGC-GCS proteins, including *Pcc*GCS, can serve as O_2 sensors, with O_2 binding resulting in increased cyclase activity [20,50,53,56]. Therefore, the O_2 dissociation rates of *Pcc*GCS variants were obtained to link the roles of heme pocket residues in signaling to their roles in O_2 binding (Fig. 1, Table 1). Both Tyr57 [29] and His112 are required for stable O_2 binding, as the Y57F and H112G variants rapidly autoxidize under aerobic conditions. The distal tyrosine and serine residues have been implicated as hydrogen bond donors in *Pcc*Globin and *Bpe*Globin, the globin domain from the DGC-GCS from *Bordatella pertussis* [52]. Specifically, the distal tyrosine serves as the primary hydrogen bond donor and has been demonstrated

Table 1
Oxygen Dissociation Rates. Errors for each rate are <5%. The two rates (k_1 and k_2) are calculated using a two exponential fit and are due to different conformations of the heme pocket.[49, 55] Representative traces and fits are shown in Fig. S3.

Protein	k_1 (s^{-1})	k_2 (s^{-1})	% k_1	% k_2
*Pcc*GCS[39]	0.56	3.87	56	44
*Pcc*GCS(Y57F)	N.A.	N.A.	N.A	N.A.
*Pcc*GCS(S82A)	1.04 ± 0.03	5.89 ± 0.11	39 ± 2	61 ± 2
*Pcc*GCS(H112G)	N.A.	N.A.	N.A	N.A.
*Pcc*GCS(V122Y)	0.70 ± 0.01	4.40 ± 0.03	65 ± 2	35 ± 2

to be essential for stabilizing bound O_2. Mutating this primary H-bonding donor, Tyr57, to phenylalanine results in immediate autoxidation upon exposure to O. In contrast, the full-length *Pcc*GCS S82A variant exhibits a slight increase in O_2 dissociation rates. This observation is in agreement with previous work on isolated globin domain variants and confirms the role of the serine -OH fragment in stabilizing bound O_2 [29]. A heme edge residue, V122, was also mutated as this position corresponds to a tyrosine in the GCSs from *B. subtilis* (HemAT-*Bs*; methyl accepting chemotaxis protein output domain) [13,14] and *P. dendritiformis* (DcpG; tandem DGC and *c*-di-GMP phosphodiesterase output domains) [24,33], both of which exhibit weak O_2 affinity and rapid O_2 dissociation. However, the *Pcc*GCS V122Y variant did not exhibit significant differences in O_2 dissociation rates as compared to WT.

In order to test the roles of heme pocket residues in DGC activation, enzyme kinetic assays were performed on *Pcc*GCS WT and full-length variants in the unbound (Fe(II)), ferrous-oxy (Fe(II)-O_2), and ferrous-nitric oxide (Fe(II)-NO) forms. The Fe(II)-NO kinetics were performed for *Pcc*GSC wild-type and all variants to allow for comparison with variants that do not stably bind O_2 (*Pcc*GCS Y57F and H112G) and therefore do not allow for measurement of O_2-dependent changes in cyclase activity. The *Pcc*GCS diguanylate cyclase kinetic parameters are shown in Table 2 and representative Michaelis-Menten plots in Fig. S3. *Pcc*GCS WT was assayed alongside all of variants as a control; *Pcc*GCS WT K_M and k_{cat} values were the same as previously reported [29,50]. Surprisingly, neither of the mutations to the distal H-bonding residues (Y57F and S82A) had a strong effect on the DGC k_{cat} and DGC fold activation (k_{cat} Fe(II)-O_2/k_{cat} Fe(II) for S82A; k_{cat} Fe(II)-NO/k_{cat} Fe(II) for Y57; Fig. 2). For both variants, the performance was nearly the same as that of *Pcc*GCS WT. However, the K_M for both variants increased compared to WT, suggesting that that the distal pocket hydrogen bonding residues are important transmitting conformational changes that stabilize GTP and O_2 binding but play little role in DGC turnover. The S82 residue also plays a role in selectivity of ligand-dependent activation of *Pcc*GCS, as the S82A variant no longer responds to NO binding. The mutation doesn't introduce any instability to the protein or the Fe(II)-NO complex, suggesting that the effects are due to interactions within the pocket. The dramatic effect of the S82A mutation on NO-dependent activation suggests that Ser82 provides the primary hydrogen bond to bound NO, either directly or through the distal pocket water [49,52]. This hydrogen bonding pattern would be analogous to one of the "closed" hydrogen bonding conformations observed in Fe(II)-O_2 HemAT-*Bs* globin [55]. The *E. coli* GCS, *Ec*DosC, only has the hydrogen bonding tyrosine (alanine is found in the analogous position of S82) and catalytic activity is also insensitive to NO binding [40], supporting our hypothesis that NO recognition requires a hydrogen bond between the secondary distal pocket hydrogen bond donor and the bound NO. (See Table 3.)

The V122Y variant yields negligible changes in k_{cat} values for all three ligation states, as shown in the Michaelis-Menten enzyme kinetic curves in Fig. S4. However, similar to the hydrogen bonding residue variants, has a larger K_M value in the Fe(II)-O_2 ligation state, resulting in lower catalytic efficiency. The H112G variant is unable to stably bind O_2 and we were unable to generate the Fe(II) unligated state of the H112G variant due to a persistent bis-imidazole ligation state (imidazole must be included in purification buffer to retain the heme). However, the Fe(II)-NO state exhibited decreased activity (k_{cat} = 0.34 min^{-1}), suggesting a possible role for the His-Fe linkage and changes in proximal helix conformation in cyclase activation.

3.1. Comparison of PccGCS full-length structure and globin domain in ferrous states, using resonance Raman spectra

To determine the effects of the middle and DGC domains on globin domain conformation, rR spectra were obtained for ferrous unligated *Pcc*GCS (the full-length protein) and the isolated globin domain, *Pcc*Globin, respectively (Fig. 3). As shown in Fig. 3A (right panel), the high-frequency rR spectrum of WT *Pcc*GCS confirms the presence of a pure ferrous form, where the oxidation state marker appears at 1354 cm^{-1}. The spin state markers, ν_3, ν_2 and ν_{10} modes, are observed at 1473, 1570 and 1612 cm^{-1}, respectively, indicating a pure five-coordinated high spin species (5cHS). The mode occurring at 1623 cm^{-1} is most reasonably assigned as the vinyl ν(C=C) mode. Interestingly, the isolated globin *Pcc*GCS exhibits a similar spectral pattern similar to that of the full-length proteins, with the band markers characteristic of a 5-coordinate high-spin (5cHS) species., i.e., the ν_3, ν_2 and ν_{10} modes occur at 1473, 1567 and 1612 cm^{-1}. Noting that a relatively intense vinyl C=C stretching mode occurs at 1619 cm^{-1}, indicating a nearly planar orientation relative to the pyrrole rings, implying enhanced conjugation.

The low-frequency region of rR spectra can offer valuable insights into the bending motions of heme peripheral groups, out-of-plane modes resulting from heme macrocycle distortions, and particularly detailed information about H-bonding interactions between bound sensor diatomic molecules and distal pocket H-bond donor residues [48,55,57–59]. Specifically, the propionate groups typically exhibit their vibrational modes in the ~360–380 cm^{-1} range, giving insights into their interactions with the protein. These interactions mainly involve hydrogen bonding and salt bridge interactions with surrounding amino acid residues, resulting in rR shifts to higher wavenumbers [60,61]. The bending modes of vinyl groups are typically observed within the 400–440 cm^{-1} region, with the lower wavenumber mode (around 410 cm^{-1}) corresponding to the in-plane orientation, while the higher wavenumber mode (approximately 440 cm^{-1}) is associated with an out-of-plane distortion [47,62].

Focusing on the low frequency rR spectrum of full length *Pcc*GCS Fig. 3A (left panel), the assigned heme skeletal modes for WT *Pcc*GCS are observed; ν_7 (670 cm^{-1}), ν_{15} (754 cm^{-1}), and ν_8 (340 cm^{-1}). The propionate modes are observed at 363 and 377 cm^{-1}, and the vinyl mode is at 410 cm^{-1}. The observation of prominent out-of-plane (OOP) modes at 305, ~487, 545, and 714 cm^{-1}, corresponding to the γ_7, γ_{12}, γ_{21}, and γ_{15} modes, respectively, indicates the characteristic "doming" OOP distortion of the heme macrocycle. This distortion is typically observed in deoxy globins, showcasing the manifestation of these modes as a hallmark feature [63]. The ν(Fe-N_{His}) for ferrous histidyl-ligated heme is typically observed in the 200 to 230 cm^{-1} spectral region [64,65]. The 229 cm^{-1} feature present in ferrous *Pcc*GCS samples suggests an iron histidine vibrational mode in this region and is found at the same wavenumber as for the *P. dendritiformis* GCS, DcpG [33]. It is

Table 2
*Pcc*GCS diguanylate cyclase kinetic parameters.

	Fe(II)			Fe(II)-O_2			Fe(II)-NO		
Protein	k_{cat} (min^{-1})	K_M (μM)	k_{cat}/ K_M $(M•min)^{-1}$	k_{cat} (min^{-1})	K_M (μM)	k_{cat}/ K_M $(M•min)^{-1}$	k_{cat} (min^{-1})	K_M (μM)	k_{cat}/ K_M $(M•min)^{-1}$
WT[39]	0.29 ± 0.01	62 ± 3	4677	0.73 ± 0.01	31 ± 6	23,548	0.51 ± 0.01	32 ± 5	15,938
Y57F	0.25 ± 0.01	85 ± 16	2941	N.A	N.A.	N.A.	0.42 ± 0.01	61 ± 9	6885
S82A	0.21 ± 0.01	145 ± 15	1448	0.52 ± 0.01	73 ± 4	7123	0.17 ± 0.05	105 ± 8	1619
H112G	N.A.	N.A.	N.A.	N.A	N.A.	N.A.	0.34 ± 0.05	127 ± 24	2677
V122Y	0.23 ± 0.01	69 ± 8	3333	0.81 ± 0.2	121 ± 21	6694	0.61 ± 0.01	36 ± 12	16,944

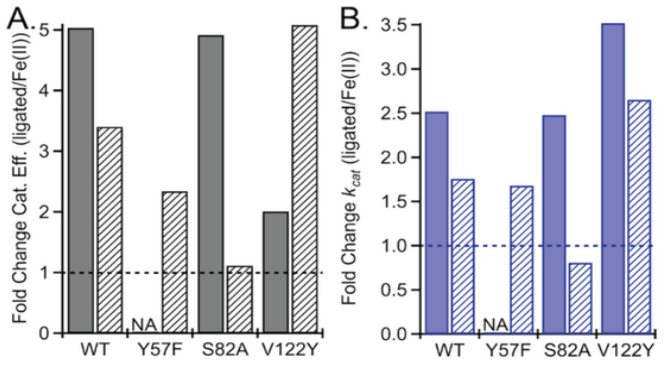

Fig. 2. Ligand-dependent fold activation on catalytic efficiency (k_{cat}/K_m; A.) and k_{cat} (B.). Solid bars correspond to activation upon O_2 binding, cross-hatched bars correspond to activation upon NO binding. Dashed horizontal lines correspond to no change in enzyme kinetics upon heme ligand binding (fold change = 1). NA, not applicable.

Table 3
The wavenumbers of ν(Fe—C) and ν(C—O) stretching modes for wild-type and *Pcc*GCS globin domains, and for their variants. The numbers in the final two columns represent the points shown in Fig. 6.

Myoglobin variants and other sensor proteins	ν(Fe—C)	ν(C—O)	Ref
FixLN CO	502	1956	[81,82]
HemAT-*Bs*	495	1966	[58,83]
CooA	487	1982	[84,85]
sGC	473	1985	[86,87]
sGC + YC-1	487	1969	[87]
Tt HNOX	490	1989	[88,89]
Tt HNOX+ YC1	489	1987	[89]
Vc HNOX	491	1985	[88,89]
NosP from *LPG*	496	1959	[71]
WT Mb	508	1941	[90]
Mb H64L	490	1968	[91]
Mb H64I	490	1968	[91]
Mb V68N	527	1922	[92]
Mb H64V/V68T	478	1983	[92]
***Pcc*GCS and variants**	ν(Fe—C)	ν(C—O)	
*Pcc*GCS FL	497	1955	This work
*Pcc*Globin	496	1956	This work
*Pcc*GCS Y57F	504	1951	This work
*Pcc*GCS S82A	497	1952	This work
*Pcc*GCS V122Y	499	1958	This work

notable that wavenumber of proximal ν(Fe-N_{his}) mode reflects its dependency on various factors. These include the H-bonding to the proximal histidine N_d hydrogen, the effect of strain from the protein on the Fe-N_{his} bond, and geometry of bound imidazole [66].

As depicted in Fig. 3B, the ferrous state rR spectra of *Pcc*Globin shows a ν(Fe-His) modes at 225 cm^{-1}, displaying a 4 cm^{-1} downshift wavenumber compared to the wild-type. This implies a potential weakening of the proximal heme Fe-N_{His} linkage, possibly due to overall conformational changes, resulting in a more labile Fe-N_{His} bond. For example, Cytochrome c peroxidase exhibits a notably higher Fe-N_{His} stretching mode at 245 cm^{-1}, attributed to the strong hydrogen bond between the axial His and the nearby Asp235 residue. Therefore, the observed downshift in Fe-N_{His} for the globin domain *Pcc*GCS suggests that the proximal histidyl fragment might adopt a less hydrogen-bonded form. Similarly, a shift in the proximal Fe-Histidine bond was observed when soluble guanylate cyclase (sGC) was truncated to the β(1–194) domain. The rR spectra indicate that ν(Fe-N_{his}) increases from 204 to 208 cm^{-1}, highlighting the importance of associated signaling components, such as methyl-accepting chemotaxis domains or diguanylate cyclase, in regulating signaling pathways [67–69].

Interestingly, the heme skeletal, out-of-plane modes, and vinyl bending modes do not significantly change when the globin domain is isolated. However, in the propionate bending mode region, while the prominent mode at 363 cm^{-1} observed in full-length *Pcc*GCS does not show significant change (365 cm^{-1} in *Pcc*Globin), the higher frequency mode at 377 cm^{-1} disappears. This implies that hydrogen bonding to the propionate groups is significantly weakened in the globin domain *Pcc*GCS. Overall, the isolation of the ferrous unligated *Pcc*GCS globin domain results in a more flexible conformation in the active site.

3.2. Comparison of PccGCS heme domains wild-type and the variants in the ferrous-unligated states

Considering the important role of heme pocket residues in DGC activation, rR spectroscopy was used to characterize the structural changes in the active site of *Pcc*Globin Y57, S82, and V122 variants. The ferrous *Pcc*GCS Y57F variant exhibits the two oxidation state marker bands, ν_4, at 1354 cm^{-1} and a small shoulder of peak at 1374 cm^{-1} in the high frequency region (Fig. 4B, right panel), indicating that the protein is in a mixture of both ferrous and ferric state;

Similarly, two ν_3 modes, observed at 1473 cm^{-1} and 1498 cm^{-1}, show that the *Pcc*Globin Y57F exists in equilibrium between five-coordinated high spin and six-coordinated low spin forms, respectively. The relative intensity of the high spin ν_3 (1473 cm^{-1}) band is larger compared to the low spin ν_3 (1498 cm^{-1}) mode, indicating higher population of high spin component. This spin state mixture is also reflected by alterations in the ν_2 and ν_{10} bands; i.e., the ν_2 bands occur at 1567 cm^{-1} and 1590 cm^{-1}, the ν_{10} bands occur at 1612 cm^{-1} and 1632 cm^{-1}. The mode occurring at 1618 cm^{-1} is most reasonably assigned as the vinyl ν(C=C) mode. The rR spectrum obtained here is consistent with previous kinetic studies, which show that the addition of O_2, either through exposure to pure O_2 gas or the addition of aerated buffer, results in rapid auto-oxidation of the heme in the Y57F variant. The failure of oxygen binding prevents the measurement of the O2 dissociation rate and O_2-dependent changes in cyclase activity. It is important to emphasize that it is unlikely that rR spectroscopy could detect a ferrous oxy species for this specific mutant. The generation of a mixture of ferric and ferrous species due to rapid auto-oxidation under aerobic conditions in this mutant further confirms the key role of Tyr57 in stable oxygen binding.

In contrast, mutating the distal site S82 residue to alanine does not induce any significant changes compared to the wild-type *Pcc*Globin, as seen in Fig. 4C (right panel); the rR spectrum exhibits characteristics of a 5cHS species, i.e., the ν_3, ν_2 and ν_{10} modes occur at 1473, 1567 and 1612 cm^{-1}. It is noted that the vinyl stretching mode is observed at 1618 cm^{-1}, quite similar to that of the WT protein. Interestingly, the rR spectrum of ferrous V122Y (Fig. 4D, right panel) exhibits the same heme markers as the wild-type and is assigned to the ferrous 5cHS species. In summary, these resonance Raman (rR) studies of the ferrous states suggest very small changes in the heme skeletal structure for these variants, findings that are in good agreement with kinetic studies. This is reflected in their similar k_{cat} and DGC fold activation compared to the wild-type proteins.

Turning attention to the low frequency rR spectra of these *Pcc*Globin variants, as shown in Fig. 5B left panels, comparing to the wild-type *Pcc*Globin, the Y57F variant does not induce significant changes in the active site pocket, exhibiting a spectrum pattern similar to that of the wild-type *Pcc*GCS. The assigned heme skeletal modes in Y57F variant are ν_7 (672 cm^{-1}), ν_{15} (754 cm^{-1}) and ν_8 (340 cm^{-1}). According to the complete assignment of other heme proteins [63,70–73], the bands observed at 363 and 377 cm^{-1} is assigned to the bending modes of the heme propionate groups, which the lower frequency indicating the disrupted H-bonding interaction with surrounding amino acid residues. The band at 412 cm^{-1} is assigned to the bending mode of the vinyl groups. Again, these distinct out-of-plane bending modes observed at

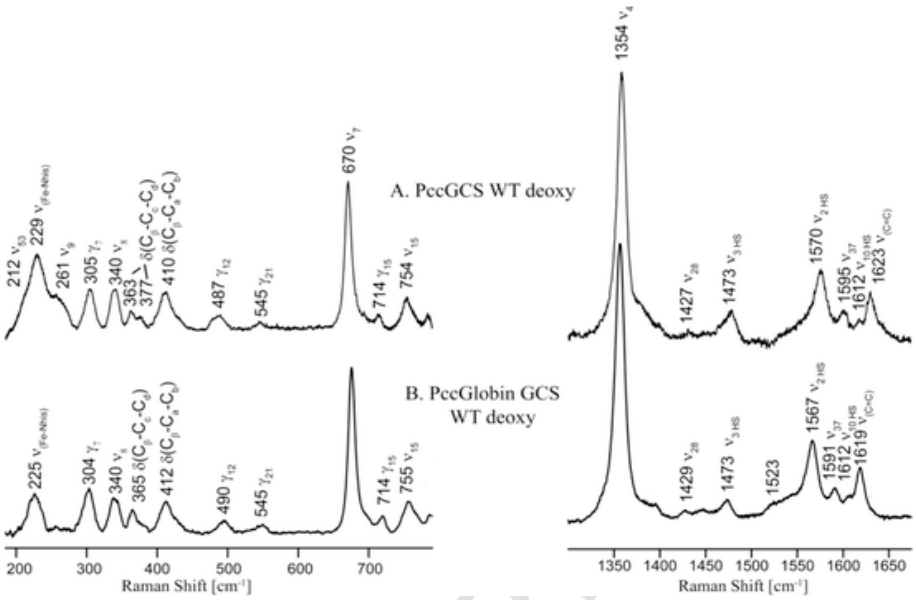

Fig. 3. rR spectra of deoxy *Pcc*GCS. The rR spectra of deoxy *Pcc*GCS (A), *Pcc*GCS Globin domain (B). Spectra were obtained using 441.6 nm excitation line. The left panel is in low frequency region, while the right panel is for high frequency. It is noted that the key ν (Fe-N_{his}) mode of *Pcc*GCS WT appearing near 229 cm^{-1} is wide and asymmetric, requiring application of the deconvolution procedures. The deconvoluted spectrum, shown in Fig. S5, helps identify the position of the Fe-Histidine band. Additionally, the mid-frequency spectra are presented in Fig. S6. These spectra exhibit no characteristic bands of sodium dithionite, confirming the absence of excess reducing agent that could disturb the spectra.

305 cm^{-1} (γ_7), 487 cm^{-1} (γ_{12}), 545 cm^{-1} (γ_{21}), and 715 cm^{-1} (γ_{15}), features characteristic of a doomed heme, similar to the wild-type *Pcc*Globin. However, it is worth noting that the ν(Fe-N_{his}) mode experiences a subtle downshift of 2 cm^{-1}, indicating that the mutation at Tyr57 slightly weakens the Fe-N_{his} bond on the proximal side, showing less strain from the protein on the Fe-N_{his} bond as a result of the overall conformational change. The *Pcc*Globin Y57F ν(Fe-N_{his}) mode is more similar to that of the *E. coli* GCS (DosC or YddV) [40], which is found at 227 cm^{-1} and *B. subtilis* (HemAT-*Bs*, 225 cm^{-1}) [59] both of which exhibit weaker O_2 affinity, as compared to *Pcc*GCS. These rR data indicate that the distal pocket hydrogen-bonding residue Y57 slightly changes the overall conformation but plays a minor role in alterations to the geometry of the heme. It is proposed that the disrupted hydrogen-bond network in the distal pocket is physiologically relevant in lowering the oxygen affinity of globin *Pcc*GCS and, therefore, stabilizing the ferrous, active form of the enzyme under aerobic conditions.

The ferrous state rR spectra of S82A variant (5B, left panel) reveals a 3 cm^{-1} downshift of the ν(Fe-N_{His}) stretching wavenumber, relative to the WT ν(Fe-His) mode at 229 cm^{-1} for WT. This observation is quite similar to the Y57F variant, again suggesting a more labile Fe-N_{his} bond, possibly caused by a conformational change. However, the mutation does not induce appreciably shift in frequencies of heme skeletal modes or the intensities of out-of-plane modes, as well as the vinyl bending mode (410 cm^{-1} in wild-type vs. 412 cm^{-1} in S82A mutant). Both proteins' vinyl groups maintain a more in-plane orientation, suggesting enhanced conjugation. Significantly, in the propionate bending mode region, the prominent mode at 363 cm^{-1} remains unaltered, while the higher frequency mode (377 cm^{-1}) disappeared, implying that hydrogen bonding to the propionate groups is significantly weakened in the S82A variant. Overall, these data indicate that ligand-dependent heme propionate movement, caused by the disruption of H bonding between Ser82 and O_2, could induce larger conformational changes in the heme active site. These changes propagate to the signaling domain through the linker region, thereby impacting the catalytic efficiency and behavior of the enzyme. These results further support a role for Ser82 in sensing O_2 binding and align with the enzyme kinetics data, which suggest that the distal hydrogen bonding network is necessary for ligand-dependent DGC activity.

Of most interest in present work is the V122Y variant. As shown in Fig. 5D (left panel), there are no significant differences in alterations to the geometry of heme peripheral groups or activation of out-of-plane modes that would reflect varying degrees of heme ruffling, which are within expectations as the V122 position does not directly interacts with the bound ligand in crystal structures of other sensor globins [30]. However, it is within Van der Waals contact the heme, it is quite interesting to see the Fe-N_{his} mode in deoxy V122Y *Pcc*GCS was significantly shifted down by 7 cm^{-1}, compared to where it was for the wild-type. This notable change in the vibrational frequency of the Fe-N_{his} mode suggests that less strain is being imposed on the Fe-N_{his} bond or less H-bonded to either a nearby proximal residue, a carbonyl group of the protein backbone, or water. These conformational changes detected by the rR data sufficiently explain the significantly larger K_m values in Fe (II)-O_2 states observed in the kinetic studies, resulting in lower catalytic efficiency. This suggests that even subtle conformational changes in the proximal pocket can lead to significant changes in enzyme functionality.

3.3. Fe – CO and CO stretching vibrations of PccGCS and heme domains Fe (II)-CO complexes

The CO adducts of heme proteins serve as valuable tools for examining the surrounding protein environment due to their chemical stability and the established correlation between their spectra and structure [74]. The CO ligand, with its vacant π* orbital, forms a linear adduct, facilitating dπ-π* overlap in perpendicular directions and thus enhancing backbonding interactions [75]. As a result, the observable ν(Fe—C) and ν(C—O) stretching modes of the Fe-C-O fragment offer insightful data on steric hindrance and hydrogen-bonding interactions affecting the Fe-C-O fragment, either by the substrate or by amino acids within the active site [76,77]. Therefore, the rR studies of ferrous CO *Pcc*Globin adducts were employed to investigate the impact of key mutations in the distal pocket on the electronic properties of heme-ligand binding.

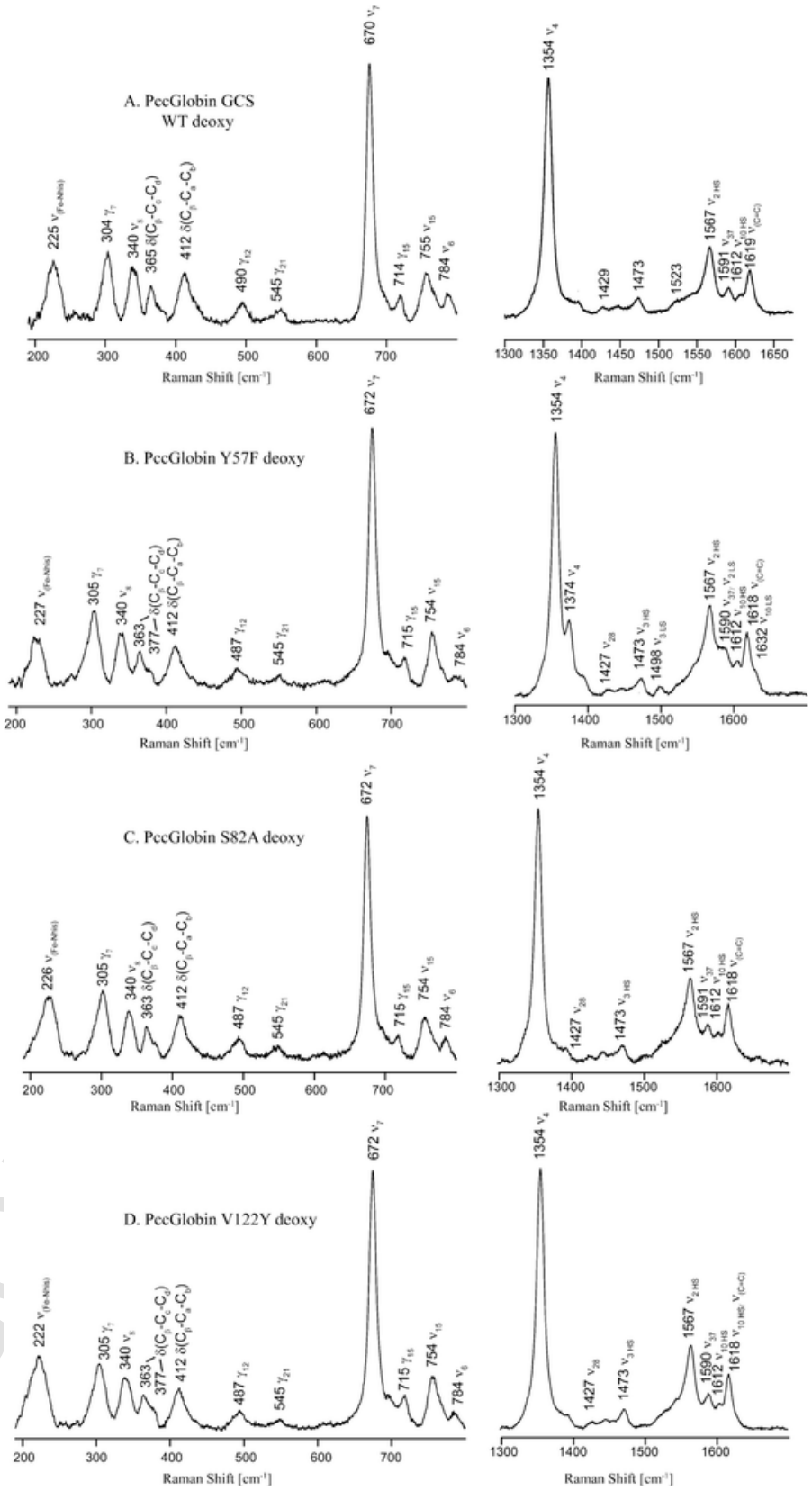

Fig. 4. rR spectra of deoxy *Pcc*GCS. The rR spectra of *Pcc*GCS Globin domain (A), *Pcc*Globin S82A (B). *Pcc*Globin Y57F (C) and *Pcc*Globin V122Y (D). Spectra were obtained using 441.6 nm excitation line. The left panel is in low-frequency region, while the right panel is for high frequency. Additionally, the mid-frequency

Fig. 4.—*continued*
spectra are shown in Fig. S6. These spectra exhibit no characteristic bands of sodium dithionite, confirming the absence of excess reducing agent that could disturb the spectra.

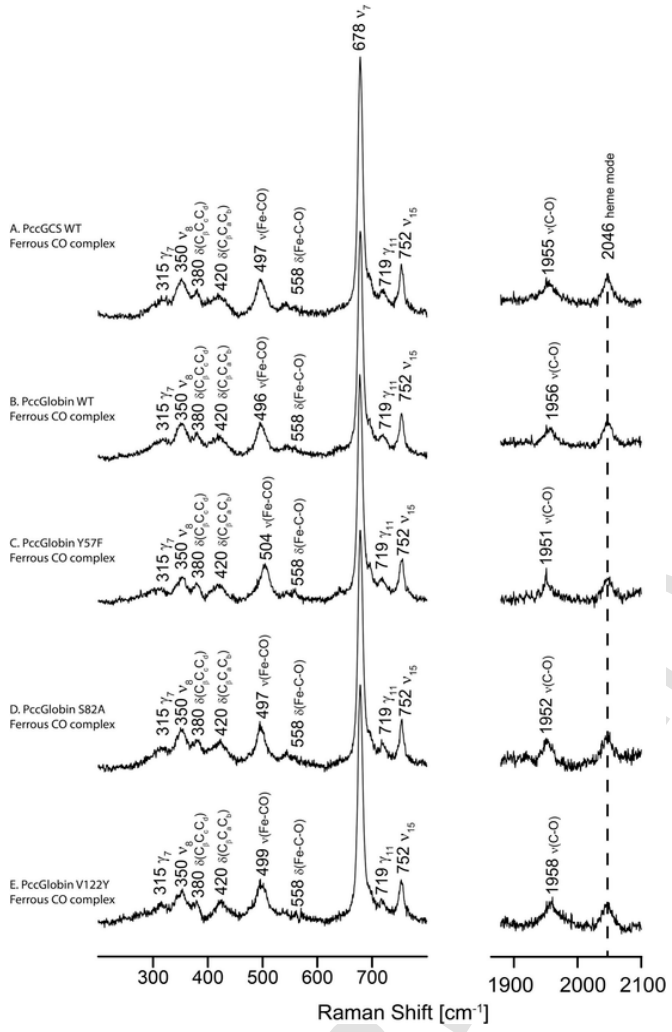

Fig. 5. The rR spectra of ferrous-CO adducts of wild-type *Pcc*GCS and their variants. The low wavenumber spectra are shown in the left-hand panels, and the high-wavenumber spectra include the C—O stretching mode in the right-hand panels. (A) wild-type *Pcc*GCS, (B) Wild-type *Pcc*Globin. (C) *Pcc*Globin Y57F variant (D) *Pcc*Globin S82A variant and (E) *Pcc*Globin V122Y variant.

The low-wavenumber rR spectra of the ferrous-CO adduct of wild-type *Pcc*GCS is shown in Fig. 5 (Trace A, left panel). The most intense band in this region, besides the ν_7 mode, is the ν(Fe—C) band seen at 497 cm^{-1}. In accordance with earlier work performed, including ^{13}CO labeling, the band at 558 cm^{-1} is assigned to the δ(Fe-C-O) bending mode, with the corresponding ν(C—O) mode occurring at 1955 cm^{-1}, as shown in Fig. 5 (Trace A, right panel). A similar spectral pattern is seen in the low-wavenumber region of the rR spectra of wild-type *Pcc*Globin (Fig. 5, trace B), where the ν(Fe—C) stretching mode occurs at 496 and the ν(C—O) mode at 1956 cm^{-1}. It is notable that these values are quite similar to the full length *Pcc*GCS (i.e., 497/1955 cm^{-1}), indicating that the active site in both forms exhibits similar polarity.

Fig. 5C-E shows the rR spectra of the ferrous-CO adduct of the *Pcc*Globin variant in both the low-wavenumber (left panel) and the high-wavenumber regions (right panel). It is important to note that these mutations have no impact on the heme core modes, including the propionate modes and the orientation of the vinyl modes (Fig. 5, left panel). In addition, all these samples exhibit a 6-coordinated low spin species, with the ν_4, ν_3, and ν_2 modes occurring at 1371, 1496 and 1580 cm^{-1}, respectively, as shown in the Fig. S7, consistent with previously published data for other heme proteins [78,79]. The absence of a band at 1358 cm^{-1}, a marker band for unligated ferrous heme, confirms that the spectra are free from contamination by modes of photodissociated species.

Specifically, attention is focused on changes in the ν(Fe-CO) and ν(C—O) modes upon these key residues that were mutated. In particular, the *Pcc*Globin Y57F ferrous-CO adduct (Fig. 5, trace C) exhibits a single ν(Fe-CO) stretching mode at 504 cm^{-1}, which is an increase of 8 cm^{-1} compared to the wild-type *Pcc*Globin. The corresponding ν(C—O) mode is observed at 1951 cm^{-1}, which is 4 wavenumbers lower in frequency relative to the wild-type protein [ν(C—O) =1955 cm^{-1}]. This is quite interesting; previous studies on myoglobin variants showed that replacing the distal histidine residue with a nonpolar residue, which cannot form H-bonding contacts with the bound CO, leads to a decreased ν(Fe—C) but an increased C—O stretching mode. Our observation is the opposite of the trends seen in myoglobin, suggesting the possibility that Tyr57 may not directly form an H-bond with the CO ligand in the native *Pcc*Globin protein, possibly mediated by a water molecule. Alternatively, the substitution of tyrosine residues with phenylalanine may have induced a conformational change in the overall structure, could cause rearrangement of the heme active site. This alteration could introduce a positive dipole, consequently lowering the C—O stretching mode while strengthening the Fe—C mode. It is important to emphasize that a decrease in C—O stretching modes is also observed in the *Tt* H-NOX Y140F and Y140L variant, but the shift is much larger (30–60 wavenumber downshift) [80]. This is because the removal of the Tyr140 residue results in the abolishment of negative polarity in the active site. It has been proposed that the distal pocket contains a localized negative polarity with the oxygen from Tyr-140 directly above the CO ligand, leading to unusually high C—O wavenumbers (~1990 cm^{-1}). Considering the C—O frequencies we observed in *Pcc*Globin are in the range of other sensor proteins [33,57,65,71], it is unlikely that Tyr57 generates the negative dipole in the active site like Tyr140 does in Tt H-NOX. These results again support the enzyme kinetics data that suggest that the Y57F mutation does not induce significant change for DGC activation.

To better understand the role of the distal H-bonding Ser-82 residue in *Pcc*Globin, the S82A variant CO complex was prepared and analyzed by rR spectroscopy. As shown in Fig. 5D, a single ν(Fe-CO) stretching mode occurs at 497 cm^{-1}, with the corresponding ν(C—O) mode being seen at 1952 cm^{-1}. The mutation has no impact on either the Fe—C frequency associated with the Fe-CO fragments or on the heme deformation modes compared to the native protein. This is consistent with the kinetic data that shows S82A plays a minor role in ligand DGC activation and fold activation. However, The C—O frequency exhibits a 4 cm^{-1} downshift, possibly resulting from the disrupted H-bonding network in the active site. These data indicate that mutations to the Ser 82 residue change the distal polarity, suggesting the role for Ser-82 in stabilizing the exogenous ligand. Fig. 5E exhibit the rR spectra of the Fe-CO complex in *Pcc*Globin V122Y variant, the ν(Fe-CO) stretching mode was observed at 499 cm^{-1} and ν(C—O) mode occurs at 1958 cm^{-1}. It is not surprising that mutating the Val122 residue to tyrosine would cause significant structural rearrangements in the active site, as reflected in the slight variations of these frequencies.

The wavenumbers of the ν(Fe—C) and ν(C—O) stretching modes for the ferrous-CO adducts of all *Pcc*Globin variants studied here are collated in Table 2. The resulting plot of ν(Fe—C) versus ν(C—O) val-

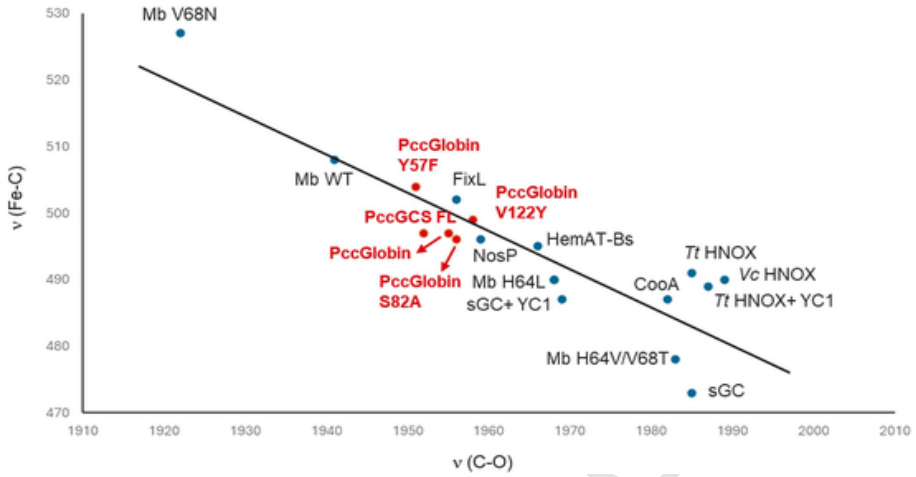

Fig. 6. Diagrams showing the inverse correlation for wild type *Pcc*GCS, PccGlobin and for their variants. The numbers represent proteins listed in Table 2. The blue circles show points for myoglobin and other sensor proteins, the red circle show points for the *Pcc*Globin proteins. (For interpretation of the references to colour in this figure legend, the reader is referred to the web version of this article.)

ues yields the anticipated inverse correlation (Fig. 6), fitting well with the line plotted for histidine-ligated 6-coordinate CO complexes [48,75]. This finding aligns with similar correlations observed in previously reported studies of myoglobin and other sensor proteins, further substantiating the consistency of this relationship across different heme proteins [74]. It is widely accepted that such correlations are primarily influenced by the polarity of the distal pocket. Positive electrostatic potentials, which are often associated with hydrogen bonding, shift the data points to the upper left, indicating enhanced Fe $d\pi \rightarrow \pi(CO)$ backbonding.

Taking the examples of myoglobin and its variants, the wild-type Mb features a distal histidine residue (H64), which engages in a weak H-bond interaction with the bound CO, resulting in a point situated midway up the backbonding line (CO = 1945 cm^{-1}) [93]. However, when H64 is substituted with a hydrophobic residue, the point shifts downward along the line (CO ~1960 cm^{-1}), suggesting a diminished polarization [77]. Conversely, distal residues that facilitate stronger H-bond interactions or possess a positive dipole are positioned higher on the line, as demonstrated by the myoglobin V68N variant [94].

Shifting our focus back to the *Pcc*GCS proteins, it is noticed that the wild-type *Pcc*GCS in both full length and isolated domain located midway of the line between these points, but are most closely to the FixL, an oxygen sensor protein possesses a relatively polar environment with distal residues (Tyr and Arg, respectively) that hydrogen bond to the coordinated gas molecule [95–97]. The data points for these globin domain variants hold the positions between the wild-type myoglobin and the H64L variants with hydrophobic replacements of the distal histidine, indicating a less polar active site environment.

4. Conclusion

In conclusion, our spectroscopic data provide valuable insights into the roles of key residues in the active site. These studies highlight the importance of distal pocket hydrogen bonding residues in modulating O_2 binding and heme pocket electronics. In addition, this work demonstrates that the second distal pocket hydrogen bonding residue, S82, is necessary for *Pcc*GCS to respond to NO binding and activate diguanylate cyclase activity. By controlling ligand binding properties and enzyme activities, the distal pocket residues dictate transmission of the O_2 binding signal within GCS proteins and to downstream signaling partners. Understanding the role of each heme pocket residue will allow for protein sequence to provide improved prediction of sensor globin characteristics and GCS function.

Funding

This work was supported by NSF CHE1352040 (E.E.W.), NSF CHE2003350 (E.E.W.), NSF CHE2312149 (E.E.W. and Y.L.), Frasch Foundation Grant 824-H17 (E.E.W.), and the start-up funds from The University of Akron (Y.L.). We thank members of the Weinert and Liu labs for assistance and helpful suggestions.

CRediT authorship contribution statement

Nushrat J. Hoque: Writing – review & editing, Formal analysis, Data curation. **Shannon Rivera:** Formal analysis, Data curation. **Paul G. Young:** Formal analysis, Data curation. **Emily E. Weinert:** Writing – review & editing, Writing – original draft, Supervision, Funding acquisition, Data curation. **Yilin Liu:** Writing – review & editing, Writing – original draft, Supervision, Funding acquisition, Data curation.

Declaration of competing interest

The authors declare that they have no known competing financial interests or personal relationships that could have appeared to influence the work reported in this paper.

Data availability

Data will be made available on request.

Acknowledgements

These studies are dedicated to the memory of Professor James Kincaid, who was not only an exceptional scientist but also a remarkable mentor and friend. Professor Kincaid's contributions to the field were profound and lasting, characterized by his innovative research and inspiring guidance. His commitment to fostering the growth of young scientists and his collegial spirit left an indelible mark on all who had the privilege to work alongside him. We honor his legacy with this work, remembering his passion for discovery and his generous mentorship.

Appendix A. Supplementary data

Supplementary data to this article can be found online at https://doi.org/10.1016/j.jinorgbio.2024.112686.

References

[1] L.J. Smith, A. Kahraman, J.M. Thornton, Heme proteins - diversity in structural characteristics, function, and folding, Proteins: Struct. Funct Bioinf. 78 (2010) 2349–2368.
[2] T.L. Poulos, Heme enzyme structure and function, Chem. Rev. 114 (2014) 3919–3962.
[3] H. Sawai, S. Yoshioka, T. Uchida, M. Hyodo, Y. Hayakawa, K. Ishimori, S. Aono (2010) Molecular oxygen regulates the enzymatic activity of a heme-containing diguanylate cyclase (HemDGC) for the synthesis of cyclic di-GMP, Biochim. Biophys. Acta 1 (1804) 166–172.
[4] N. Muraki, C. Kitatsuji, S. Aono, A new biological function of heme as a signaling molecule, J. Porphyrins Phthalocyanines 19 (2015) 9–20.
[5] H.M. Girvan, A.W. Munro, Heme sensor proteins, J. Biol. Chem. 288 (2013) 13194–13203.
[6] T. Uchida, T. Kitagawa, Mechanism for transduction of the ligand-binding signal in heme-based gas sensory proteins revealed by resonance Raman spectroscopy, Acc. Chem. Res. 38 (2005) 662–670.
[7] S.F. EI-Mashtoly, T. Kitagawa, Structural chemistry involved in information detection and transmission by gas sensor heme proteins: resonance Raman investigation, Pure Appl. Chem. 80 (2008) 2667–2678.
[8] S. Aono, Metal-containing sensor proteins sensing diatomic gas molecules, Dalton T (2008) 3137–3146.
[9] M. Martinkova, K. Kitanishi, T. Shimizu, Heme-based globin-coupled oxygen sensors: linking oxygen binding to functional regulation of diguanylate cyclase, histidine kinase and methyl-accepting chemotaxis, J. Biol. Chem. 288 (2013) 27702–27711.
[10] T. Shimizu, D. Huang, F. Yan, M. Stranava, M. Bartosova, V. Fojtíková, M. Martínková, Gaseous O2, NO, and CO in signal transduction: structure and function relationships of heme-based gas sensors and heme-redox sensors, Chem. Rev. 115 (2015) 6491–6533.
[11] N.J. Hoque, E.E. Weinert, Control of bacterial second messenger signaling and motility by heme-based direct oxygen-sensing proteins, Curr. Opin. Microbiol. 76 (2023) 102396.
[12] J.A. Walker, S. Rivera, E.E. Weinert, Mechanism and role of globin coupled sensor signaling, Adv. Microb. Physiol. 71 (2017) 133–169.
[13] W. Zhang, G.N. Phillips Jr, Structure of the oxygen sensor in *Bacillus subtilis*: signal transduction of chemotaxis by control of symmetry, Structure 11 (2003) 1097–1110.
[14] W. Zhang, J.S. Olson, G.N. Phillips Jr, Biophysical and kinetic characterization of HemAT, an aerotaxis receptor from Bacillus subtilis, Biophys. J. 88 (2005) 2801–2814.
[15] S. Hou, R.W. Larsen, D. Boudko, C.W. Riley, E. Karatan, M. Zimmer, G.W. Ordal, M. Alam, Myoglobin-like aerotaxis transducers in archaea and bacteria, Nature 403 (2000) 540–544.
[16] V. Fojtikova, M. Stranava, M.H. Vos, U. Liebl, J. Hranicek, K. Kitanishi, T. Shimizu, M. Martinkova, Kinetic analysis of a globin-coupled histidine kinase, AfGcHK: effects of the heme iron complex, response regulator, and metal cations on autophosphorylation activity, Biochemistry 54 (2015) 5017–5029.
[17] K. Kitanishi, K. Kobayashi, T. Uchida, K. Ishimori, J. Igarashi, T. Shimizu, Identification and functional and spectral characterization of a globin-coupled histidine kinase from Anaeromyxobacter sp. Fw109-5, J. Biol. Chem. 286 (2011) 35522–35534.
[18] M. Stranava, V. Martínek, P. Man, V. Fojtikova, D. Kavan, O. Vaněk, T. Shimizu, M. Martinkova, Structural characterization of the heme-based oxygen sensor, AfGcHK, its interactions with the cognate response regulator, and their combined mechanism of action in a bacterial two-component signaling system, Proteins 84 (2016) 1375–1389.
[19] J.L. Burns, D. Douglas Deer, E.E. Weinert, Oligomeric state affects oxygen dissociation and diguanylate cyclase activity of globin coupled sensors, Mol. BioSyst. 10 (2014) 2823–2826.
[20] K. Kitanishi, K. Kobayashi, Y. Kawamura, I. Ishigami, T. Ogura, K. Nakajima, J. Igarashi, A. Tanaka, T. Shimizu, Important roles of Tyr43 at the putative heme distal side in the oxygen recognition and stability of the Fe(II)-O2 complex of YddV, a globin-coupled heme-based oxygen sensor diguanylate cyclase, Biochemistry 49 (2010) 10381–10393.
[21] J.R. Tuckerman, G. Gonzalez, E.H. Sousa, X. Wan, J.A. Saito, M. Alam, M.A. Gilles-Gonzalez, An oxygen-sensing diguanylate cyclase and phosphodiesterase couple for c-di-GMP control, Biochemistry 48 (2009) 9764–9774.
[22] C. Wu, Y.Y. Cheng, H. Yin, X.N. Song, W.W. Li, X.X. Zhou, L.P. Zhao, L.J. Tian, J.C. Han, H.Q. Yu, Oxygen promotes biofilm formation of Shewanella putrefaciens CN32 through a diguanylate cyclase and an adhesin, Sci. Rep. 3 (2013) 1945–1951.
[23] H. Sawai, S. Yoshioka, T. Uchida, M. Hyodo, Y. Hayakawa, K. Ishimori, S. Aono, Molecular oxygen regulates the enzymatic activity of a heme-containing diguanylate cyclase (HemDGC) for the synthesis of cyclic di-GMP, Biochim. Biophys. Acta 1804 (2010) 166–172.
[24] D.C. Patterson, M.P. Ruiz, H. Yoon, J.A. Walker, J.P. Armache, N.H. Yennawar, E.E. Weinert, Differential ligand-selective control of opposing enzymatic activities within a bifunctional c-di-GMP enzyme, Proc. Natl. Acad. Sci. USA 118 (2021).
[25] K. Kitanishi, N. Aoyama, M. Shimonaka, Gas-selective catalytic regulation by a newly identified globin-coupled sensor phosphodiesterase containing an HD-GYP Domain from the human pathogen Vibrio fluvialis, Biochemistry 63 (2024) 523–532.
[26] A. Lengalova, V. Fojtikova-Proskova, J. Vavra, V. Martinek, M. Stranava, T. Shimizu, M. Martinkova, Kinetic analysis of a globin-coupled diguanylate cyclase, YddV: Effects of heme iron redox state, axial ligands, and heme distal mutations on catalysis, J. Inorg. Biochem. 201 (2019) 110833.
[27] J.R. Tuckerman, G. Gonzalez, M.A. Gilles-Gonzalez, Cyclic di-GMP activation of polynucleotide phosphorylase signal-dependent RNA processing, J. Mol. Biol. 407 (2011) 633–639.
[28] J.L. Burns, S. Rivera, D.D. Deer, S.C. Joynt, D. Dvorak, E.E. Weinert, Oxygen and c-di-GMP binding control oligomerization state equilibria of diguanylate cyclase-containing globin coupled sensors, Biochemistry 55 (2016) 6642–6651.
[29] S. Rivera, J.L. Burns, G.E. Vansuch, B. Chica, E.E. Weinert, Globin domain interactions control heme pocket conformation and oligomerization of globin coupled sensors, J. Inorg. Biochem. 164 (2016) 70–76.
[30] S. Rivera, P.G. Young, E.D. Hoffer, G.E. Vansuch, C.L. Metzler, C.M. Dunham, E.E. Weinert, Structural insights into oxygen-dependent signal transduction within globin coupled sensors, Inorg. Chem. 57 (2018) 14386–14395.
[31] J.A. Walker, Y. Wu, J.R. Potter, E.E. Weinert, pi-helix controls activity of oxygen-sensing diguanylate cyclases, Biosci. Rep. 40 (2020) BSR20193602.
[32] A. Schuelke-Sanchez, N.H. Yennawar, E.E. Weinert, Oxygen-selective regulation of cyclic di-GMP synthesis by a globin coupled sensor with a shortened linking domain modulates Shewanella sp. ANA-3 biofilm, J. Inorg. Biochem. 252 (2024) 112482.
[33] D.C. Patterson, Y. Liu, S. Das, N.H. Yennawar, J.-P. Armache, J.R. Kincaid, E.E. Weinert, Heme-edge residues modulate signal transduction within a bifunctional homo-dimeric sensor protein, Biochemistry 60 (49) (2021) 3801–3812.
[34] A. Deepthi, C.W. Liew, Z.X. Liang, K. Swaminathan, J. Lescar, Structure of a diguanylate cyclase from Thermotoga maritima: insights into activation, feedback inhibition and thermostability, PLoS ONE 9 (2014) e110912.
[35] R. Hengge, High-specificity local and global c-di-GMP signaling, Trends Microbiol. 29 (2021) 993–1003.
[36] R. Hengge, Principles of c-di-GMP signalling in bacteria, Nat. Rev. Microbiol. 7 (2009) 263–273.
[37] U. Römling, Cyclic di-GMP signaling-where did you come from and where will you go? Mol. Microbiol. 120 (2023) 564–574.
[38] U. Römling, M.Y. Galperin, M. Gomelsky, Cyclic di-GMP: the first 25 years of a universal bacterial second messenger, Microbiol. Mol. Biol. Rev. 77 (2013) 1–52.
[39] J.L. Burns, D.D. Deer, E.E. Weinert, Oligomeric state affects oxygen dissociation and diguanylate cyclase activity of globin coupled sensors, Mol. BioSyst. 10 (2014) 2823–2826.
[40] K. Kitanishi, K. Kobayashi, Y. Kawamura, I. Ishigami, T. Ogura, K. Nakajima, J. Igarashi, A. Tanaka, T. Shimizu, Important roles of Tyr43 at the putative heme distal side in the oxygen recognition and stability of the Fe(II)-O2 complex of YddV, a globin-coupled heme-based oxygen sensor diguanylate cyclase, Biochemistry 49 (2010) 10381–10393.
[41] C. Wu, Y.Y. Cheng, H. Yin, X.N. Song, W.W. Li, X.X. Zhou, L.P. Zhao, L.J. Tian, J.C. Han, H.Q. Yu, Oxygen promotes biofilm formation of Shewanella putrefaciens CN32 through a diguanylate cyclase and an adhesin, Sci. Rep. 3 (2013) 1945.
[42] T.G. Spiro, Resonance raman spectroscopy: a new structure probe for biological chromophores, Reson. Raman Spectrosc. 7 (1974) 6.
[43] T.G. Spiro, Biological Application of Raman Spectroscopy, 3, Wiley, New York, 1988.
[44] T. Kitagawa, Y. Mizutani, Resonance Raman-spectra of highly oxidized metalloporphyrins and heme-proteins, Coord. Chem. Rev. 135 (1994) 685–735.
[45] L.S. Reid, M.R. Mauk, A.G. Mauk, Role of heme propionate groups in cytochrome-b5 electron-transfer, J. Am. Chem. Soc. 106 (1984) 2182–2185.
[46] L.S. Reid, A.R. Lim, A.G. Mauk, Role of heme vinyl groups in cytochrome-B5 electron-transfer, J. Am. Chem. Soc. 108 (1986) 8197–8201.
[47] K.B. Lee, E.S. Jun, G.N. Lamar, I.N. Rezzano, R.K. Pandey, K.M. Smith, F.A. Walker, D.H. Buttlaire, Influence of heme vinyl-protein and carboxylate protein contacts on structure and redox properties of bovine cytochrome-B5, J. Am. Chem. Soc. 113 (1991) 3576–3583.
[48] T.G. Spiro, A.V. Soldatova, G. Balakrishnan, CO, NO and O-2 as vibrational probes of heme protein interactions, Coord. Chem. Rev. 257 (2013) 511–527.
[49] S. Rivera, P.G. Young, E.D. Hoffer, G.E. Vansuch, C.L. Metzler, C.M. Dunham, E.E. Weinert, Structural insights into oxygen-dependent signal transduction within globin coupled sensors, Inorg. Chem. 57 (2018) 14386–14395.
[50] J.L. Burns, D. Douglas Deer, E.E. Weinert, Oligomeric state affects oxygen dissociation and diguanylate cyclase activity of globin coupled sensors, Mol. BioSyst. 10 (2014) 2823–2826.
[51] N.J. Hoque, M.P. Helm, E.E. Weinert, In vitro measurement of gas-dependent and redox-sensitive diguanylate cyclase activity, Methods Mol. Biol. 2648 (2023) 75–86.
[52] S. Rivera, J.L. Burns, G.E. Vansuch, B. Chica, E.E. Weinert, Globin domain interactions control heme pocket conformation and oligomerization of globin coupled sensors, J. Inorg. Biochem. 164 (2016) 70–76.
[53] X. Wan, J.R. Tuckerman, J.A. Saito, T.A. Freitas, J.S. Newhouse, J.R. Denery, M.Y. Galperin, G. Gonzalez, M.A. Gilles-Gonzalez, M. Alam, Globins synthesize the second messenger bis-(3'-5')-cyclic diguanosine monophosphate in bacteria, J. Mol. Biol. 388 (2009) 262–270.
[54] E.E. Weinert, L. Plate, C.A. Whited, C. Olea Jr, M.A. Marletta, Determinants of ligand affinity and heme reactivity in H-NOX domains, Angew. Chem. Int. Ed. Eng. 49 (2010) 720–723.

[55] T. Ohta, H. Yoshimura, S. Yoshioka, S. Aono, T. Kitagawa, Oxygen-sensing mechanism of HemAT from Bacillus subtilis: a resonance Raman spectroscopic study, J. Am. Chem. Soc. 126 (2004) 15000–15001.
[56] H. Sawai, S. Yoshioka, T. Uchida, M. Hyodo, Y. Hayakawa, K. Ishimori, S. Aono, Molecular oxygen regulates the enzymatic activity of a heme-containing diguanylate cyclase (HemDGC) for the synthesis of cyclic di-GMP, Biochim. Biophys. Acta 1804 (2010) 166–172.
[57] Y. Liu, J.R. Kincaid, Resonance Raman studies of gas sensing heme proteins, J. Raman Spectrosc. 52 (2021) 20.
[58] H. Yoshimura, S. Yoshioka, K. Kobayashi, T. Ohta, T. Uchida, M. Kubo, T. Kitagawa, S. Aono, Specific hydrogen-bonding networks responsible for selective O2 sensing of the oxygen sensor protein HemAT from Bacillus subtilis, Biochemistry 45 (2006) 8301–8307.
[59] S. Aono, T. Kato, M. Matsuki, H. Nakajima, T. Ohta, T. Uchida, T. Kitagawa, Resonance Raman and ligand binding studies of the oxygen-sensing signal transducer protein HemAT from Bacillus subtilis, J. Biol. Chem. 277 (2002) 13528–13538.
[60] E.S. Peterson, J.M. Friedman, E.Y.T. Chien, S.G. Sligar, Functional implications of the proximal hydrogen-bonding network in myoglobin: a resonance Raman and kinetic study of Leu89, Ser92, His97, and F-helix swap mutants, Biochemistry 37 (1998) 12301–12319.
[61] J.F. Cerda-Colon, E. Silfa, J. Lopez-Garriga, Unusual rocking freedom of the heme in the hydrogen sulfide-binding hemoglobin from Lucina pectinata, J. Am. Chem. Soc. 120 (1998) 9312–9317.
[62] Z. Chen, T.W. Ost, J.P. Schelvis, Phe393 mutants of cytochrome P450 BM3 with modified heme redox potentials have altered heme vinyl and propionate conformations, Biochemistry 43 (2004) 1798–1808.
[63] F. Rwere, P.J. Mak, J.R. Kincaid, Resonance Raman interrogation of the consequences of heme rotational disorder in myoglobin and its ligated derivatives, Biochemistry 47 (2008) 12869–12877.
[64] B. Pal, T. Kitagawa, Interactions of soluble guanylate cyclase with diatomics as probed by resonance Raman spectroscopy, J. Inorg. Biochem. 99 (2005) 267–279.
[65] E. Martin, K. Czarnecki, V. Jayaraman, F. Murad, J. Kincaid, Resonance Raman and infrared spectroscopic studies of high-output forms of human soluble guanylyl cyclase, J. Am. Chem. Soc. 127 (2005) 4625–4631.
[66] E.S. Peterson, J.M. Friedman, E.Y.T. Chien, S.G. Sligar, Functional implications of the proximal hydrogen-bonding network in myoglobin: a resonance raman and kinetic study of Leu89, Ser92, His97, and F-helix swap mutants, Biochemistry 37 (1998) 12301–12319.
[67] D.S. Karow, D. Pan, J.H. Davis, S. Behrends, R.A. Mathies, M.A. Marletta, Characterization of functional heme domains from soluble guanylate cyclase, Biochemistry 44 (2005) 16266–16274.
[68] Y. Zhao, J.P.M. Schelvis, G.T. Babcock, M.A. Marletta, Identification of histidine 105 in the β1 subunit of soluble guanylate cyclase as the heme proximal ligand, Biochemistry 37 (1998) 4502–4509.
[69] J.P.M. Schelvis, Y. Zhao, M.A. Marletta, G.T. Babcock, Resonance Raman characterization of the heme domain of soluble guanylate cyclase, Biochemistry 37 (1998) 16289–16297.
[70] Y. Liu, K.J. McLean, A.W. Munro, J.R. Kincaid, Resonance Raman studies of Bacillus megaterium cytochrome P450 BM3 and biotechnologically important mutants, J. Raman Spectrosc. 49 (2018) 287–297.
[71] B.A. Bacon, Y. Liu, J.R. Kincaid, E.M. Boon, Spectral characterization of a novel NO sensing protein in bacteria: NosP, Biochemistry 57 (2018) 6187–6200.
[72] F. Rwere, P.J. Mak, J.R. Kincaid, The impact of altered protein-heme interactions on the resonance raman spectra of heme proteins. Studies of heme rotational disorder, Biopolymers 89 (2008) 179–186.
[73] P.J. Mak, D. Kaluka, M.E. Manyumwa, H. Zhang, T. Deng, J.R. Kincaid, Defining resonance Raman spectral responses to substrate binding by cytochrome P450 from Pseudomonas putida, Biopolymers 89 (2008) 1045–1053.
[74] T.G. Spiro, I.H. Wasbotten, CO as a vibrational probe of heme protein active sites, J. Inorg. Biochem. 99 (2005) 34–44.
[75] X.Y. Li, T.G. Spiro, Is bound co linear or bent in heme-proteins - evidence from resonance Raman and infrared spectroscopic data, J. Am. Chem. Soc. 110 (1988) 6024–6033.
[76] M. Ibrahim, C.L. Xu, T.G. Spiro, Differential sensing of protein influences by NO and CO vibrations in heme adducts, J. Am. Chem. Soc. 128 (2006) 16834–16845.
[77] T. Uno, Y. Nishimura, R. Makino, T. Iizuka, Y. Ishimura, M. Tsuboi, The resonance Raman frequencies of the Fe-Co stretching and bending modes in the Co complex of cytochrome P-450cam, J. Biol. Chem. 260 (1985) 2023–2026.
[78] P.J. Mak, S.C. Im, H.M. Zhang, L.A. Waskell, J.R. Kincaid, Resonance Raman studies of cytochrome P4502B4 in its interactions with substrates and redox partners, Biochemistry 47 (2008) 3950–3963.
[79] P.J. Mak, M.C. Gregory, S.G. Sligar, J.R. Kincaid, Resonance Raman spectroscopy reveals that substrate structure selectively impacts the heme-bound diatomic ligands of CYP17, Biochemistry 53 (2014) 90–100.
[80] R. Tran, E.E. Weinert, E.M. Boon, R.A. Mathies, M.A. Marletta, Determinants of the heme-CO vibrational modes in the H-NOX family, Biochemistry 50 (2011) 6519–6530.
[81] K.R. Rodgers, G.S. Lukat-Rodgers, J.A. Barron, Structural basis for ligand discrimination and response initiation in the heme-based oxygen sensor FixL, Biochemistry 35 (1996) 9539–9548.
[82] H. Miyatake, M. Mukai, S.-I. Adachi, H. Nakamura, K. Tamura, T. Iizuka, Y. Shiro, R.W. Strange, S.S. Hasnain, Iron coordination structures of oxygen sensor FixL characterized by Fe K-edge extended x-ray absorption fine structure and resonance Raman spectroscopy, J. Biol. Chem. 274 (1999) 23176–23184.
[83] S. Aono, T. Kato, M. Matsuki, H. Nakajima, T. Ohta, T. Uchida, T. Kitagawa, Resonance Raman and ligand binding studies of the oxygen-sensing signal transducer protein HemAT from Bacillus subtilis, J. Biol. Chem. 277 (2002) 13528–13538.
[84] C.M. Coyle, M. Puranik, H. Youn, S.B. Nielsen, R.D. Williams, R.L. Kerby, G.P. Roberts, T.G. Spiro, Activation mechanism of the CO sensor CooA: mutational and resonance Raman spectroscopic studies, J. Biol. Chem. 278 (2003) 35384–35393.
[85] K.M. Vogel, T.G. Spiro, D. Shelver, M.V. Thorsteinsson, G.P. Roberts, Resonance Raman evidence for a novel charge relay activation mechanism of the CO-dependent heme protein transcription factor CooA, Biochemistry 38 (1999) 2679–2687.
[86] G. Deinum, J.R. Stone, G.T. Babcock, M.A. Marletta, Binding of nitric oxide and carbon monoxide to soluble guanylate cyclase as observed with resonance Raman spectroscopy, Biochemistry 35 (1996) 1540–1547.
[87] M. Ibrahim, E.R. Derbyshire, M.A. Marletta, T.G. Spiro, Probing soluble guanylate cyclase activation by CO and YC-1 using resonance Raman spectroscopy, Biochemistry 49 (2010) 3815–3823.
[88] D.S. Karow, D. Pan, R. Tran, P. Pellicena, A. Presley, R.A. Mathies, M.A. Marletta, Spectroscopic characterization of the soluble guanylate cyclase-like Heme domains from Vibrio cholerae and thermoanaerobacter tengcongensis, Biochemistry 43 (2004) 10203–10211.
[89] E.R. Derbyshire, M.B. Winter, M. Ibrahim, S. Deng, T.G. Spiro, M.A. Marletta, Probing domain interactions in soluble guanylate cyclase, Biochemistry 50 (2011) 4281–4290.
[90] T. Li, M.L. Quillin, G.N. Phillips Jr, J.S. Olson, Structural determinants of the stretching frequency of CO bound to myoglobin, Biochemistry 33 (1994) 1433–1446.
[91] J. Ling, T. Li, J.S. Olson, D.F. Bocian, Identification of the iron-carbonyl stretch in distal histidine mutants of carbonmonoxymyoglobin, Biochim. Biophys. Acta Bioenerg. 1188 (1994) 417–421.
[92] C.L. Anderton, R.E. Hester, J.N. Moore, A chemometric analysis of the resonance Raman spectra of mutant carbonmonoxy-myoglobins reveals the effects of polarity, Biochim. Biophys. Acta Protein Struct. Mol. Enzymol. 1338 (1997) 107–120.
[93] M. Unno, J.F. Christian, J.S. Olson, J.T. Sage, P.M. Champion, Evidence for hydrogen bonding effects in the iron ligand vibrations of carbonmonoxy myoglobin, J. Am. Chem. Soc. 120 (1998) 2670–2671.
[94] T.K. Das, J.M. Friedman, A.P. Kloek, D.E. Goldberg, D.L. Rousseau, Origin of the anomalous Fe-CO stretching mode in the CO complex of ascaris hemoglobin, Biochemistry 39 (2000) 837–842.
[95] Miyatake, H., Mukai, M., Park, S.-Y., Adachi, S.-i., Tamura, K., Nakamura, H., Nakamura, K., Tsuchiya, T., Iizuka, T., and Shiro, Y. (2000) Sensory mechanism of oxygen sensor FixL from Rhizobium meliloti: crystallographic, mutagenesis and resonance raman spectroscopic studies11Edited by K, Nagai. J. Mol. Biol. 301, 415-431.
[96] W. Gong, B. Hao, S.S. Mansy, G. Gonzalez, M.A. Gilles-Gonzalez, M.K. Chan, Structure of a biological oxygen sensor: a new mechanism for heme-driven signal transduction, Proc. Natl. Acad. Sci. 95 (1998) 15177–15182.
[97] P. Nioche, V. Berka, J. Vipond, N. Minton, A.L. Tsai, C.S. Raman, Femtomolar sensitivity of a NO sensor from Clostridium botulinum, Science 306 (2004) 1550–1553.